# Ab Initio Study of Proton Transfer and Interfacial Properties in Phosphoric Acid-Doped Polybenzimidazole

**ARTICLE** *in* MACROMOLECULAR THEORY AND SIMULATIONS · SEPTEMBER 2013

Impact Factor: 1.67 · DOI: 10.1002/mats.201300002



**2 AUTHORS:**

Shuo Li
Procter & Gamble
**10** PUBLICATIONS **177** CITATIONS
SEE PROFILE

Joel Fried
University of Louisville
**145** PUBLICATIONS **1,589** CITATIONS
SEE PROFILE

# Ab Initio Study of Proton Transfer and Interfacial Properties in Phosphoric Acid-Doped Polybenzimidazole

Shuo Li, J. R. Fried*

Quantum mechanics calculations and hybrid ab initio/empirical molecular dynamics simulations using the ONIOM scheme have been used to investigate proton transfer and interfacial properties in phosphoric acid (PA)-doped polybenzimidazole. Quantum mechanics calculations indicate that hydrogen bonding between PA and benzimidazole (with PA as the hydrogen donor) is the major interaction between PA and polybenzimidazole at low PA-doping levels. Comparing energy barriers for different proton transfer pathways indicates that proton transfer is prone to occur between the same molecules or between a molecule and its corresponding ion. The atom-centered density matrix propagation approach coupled with ONIOM using density functional theory and universal force field calculations indicates that protonation of the "=N–" atom on the imidazole ring occurs when there are two or more PA molecules surrounding each imidazole ring. These conclusions agree with the experimental results in the literature.

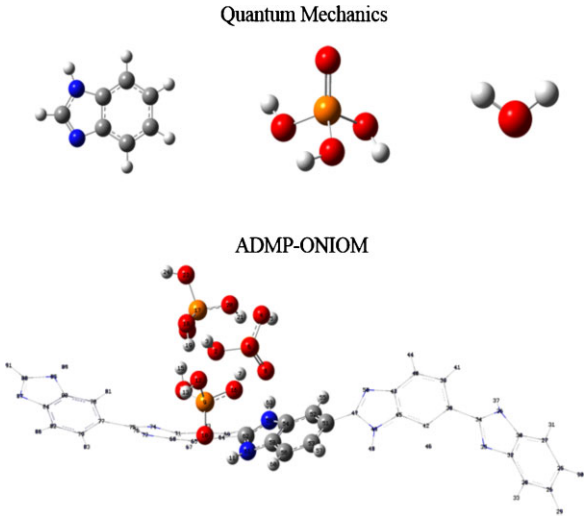


## 1. Introduction

Proton transfer (PT) is the essential process in proton-exchange membranes for fuel cell applications where high proton conductivity is the controlling property and, therefore, a fundamental understanding of the PT mechanisms is critical to the continuing development of proton exchange membrane fuel cells. Generally, PT can be described as a combination of proton hopping along the hydrogen-bonded network (also known as "structural diffusion" by the Grotthuss mechanism[1]) and the diffusion of proton carriers between hops (also known as "vehicular diffusion"). Structural diffusion occurs over small time scales (up to a few picoseconds), whereas vehicular diffusion occurs at a larger time scale (i.e., nanoseconds).[2] Both mechanisms are known to contribute to PT.[3,4] Multi-scale simulations can provide insight into the nature of these mechanisms and to evaluate contributions from different mechanisms to the overall PT efficiency.

Among candidates for proton-exchange membranes, Nafion®[5] has been most extensively studied. Nafion is composed of a hydrophobic perfluorinated alkane backbone and a strongly hydrophilic sulfonic acid-terminated

S. Li, J. R. Fried
Department of Chemical Engineering, University of Cincinnati, Cincinnati, OH 45221-0012, USA
Fax: +937 229 3433; E-mail: jfried1@udayton.edu
Current address: Chemical and Materials Engineering, University of Dayton, Dayton OH 45469-0240, USA




DOI: 10.1002/mats.201300002

perfluorovinyl ether side chain. Its high proton conductivity (0.13 $S \cdot cm^{-1}$ at 75 °C) depends on content of water that facilitates proton dissociation from the sulfonic acid group and serves as shuttles for PT.[6,7] Multi-scale modeling techniques have been used to investigate PT and the hydrogen bonding in Nafion membranes. Techniques include quantum mechanics,[8,9] ab initio molecular dynamics[10–14] and metadynamics,[15] empirical valence bond methodology,[16–18] statistical mechanics,[19] classical,[2,20–23] and mesoscale molecular dynamics.[24,25] Most of these approaches have been recently reviewed by Elliott and Paddison[26] and Devanathan.[6]

Unfortunately, the high water dependency of Nafion limits its working temperature to 100 °C.[27,28] The advantages of the high-temperature operation of fuel cells have been summarized in several review papers.[27–29] Important advantages include increased electrode tolerance at elevated temperatures and improved efficiency. For these reasons, significant effort has been devoted to developing novel membrane materials that can work at higher temperatures. One approach is the use of anhydrous membranes that use a high-boiling-point liquid in place of water as the proton medium.[2] Polybenzimidazoles are linear aromatic polymers that exhibit excellent mechanical strength, thermal and chemical stability, and high ionic conductivity when doped with acid.[30] Xing and Savadogo[31] have compared the conductivity of polybenzimidazole membranes doped with different acid, and concluded that the conductivity changes in the order $H_2SO_4 > H_3PO_4 > HClO_4 > HNO_3 > HCl$ at high doping levels. However, phosphoric acid (PA)-doped polybenzimidazoles exhibit the highest thermal stability and are therefore studied most broadly.[32] PA is amphoteric, containing both proton donor and acceptor groups to form dynamic hydrogen bond networks, where PT occurs during the hydrogen bond breaking and forming processes.[28] At its melting temperature ($T_m$) of 42 °C, the conductivity of neat PA can reach $7.7 \times 10^{-2}$ $S \cdot cm^{-1}$, with an estimated proton mobility of $2 \times 10^{-5}$ $cm^2 \cdot s^{-1}$ according to the Nernst–Einstein equation.[3,33] This is similar to the self-diffusion coefficient of water at room temperature ($2.25 \times 10^{-5}$ $cm^2 \cdot s^{-1}$).[3] This high conductivity makes PA suitable for applications as an individual electrolyte in liquid fuel cells[34] as well as a dopant in proton-exchange membranes (e.g., polybenzimidazoles).[35]

In the recent years, extensive research activities have been motivated in the laboratory to further improve PA-doped polybenzimidazole membranes, in order to reach higher conductivity while maintaining good mechanical/thermal stability in the temperature range of 120–200 °C. As generally agreed, the membrane conductivity depends on the doping level of PA, temperature, and relative humidity;[27,28,36,37] however, the underlying PT mechanisms are still unclear. Laboratory techniques including Infrared,[38–43] Raman,[41,44] and nuclear magnetic resonance spectra[42,43] have indicated strong hydrogen bonding between PA and the nitrogen atoms on the imidazole rings of polybenzimidazoles, resulting in the formation of $H_2PO_4^-$.[28] Ma et al.[37] measured the conductivity of PA-doped polybenzimidazoles at different acid doping levels and proposed that the rate of PT between different species follows the order $H_3PO_4$ $(H_2PO_4^-)\ldots H{-}O{-}H > H_3PO_4\ldots H_2PO_4^- > N{-}H^+\ldots H_2PO_4^- > N{-}H^+\ldots H{-}O{-}H > N{-}H^+\ldots N{-}H$. He et al.[45] also used the Scatchard[46] method to calculate the interaction between acid and the two "N" binding sites on the imidazole ring at varied acid doping levels and reached similar conclusions as reached by Ma et al.[37]

There have only been a few reported simulation studies of PA-doped polybenzimidazoles. Only our group,[47,48] Zhu et al.[49], and Pahari et al.[50] have used classical molecular dynamics simulations to model the hydrogen bond network and vehicular diffusion in PA-doped polybenzimidazole systems at the timescale of nanoseconds. In these published studies, the structural diffusion of protons is completely neglected due to the inability of classical molecular dynamics to describe bond-breaking and bond-making events; however, structural diffusion is known to make a greater contribution to the overall proton conductivity than does vehicular diffusion in most cases.[3] In this communication, quantum mechanics calculations and hybrid ab initio/empirical molecular dynamics simulations using the ONIOM Scheme [51,52] have been used to investigate structural diffusion and interfacial properties between PA and polybenzimidazoles. First, proton affinity, interaction energy, and energy barriers for different PT pathways were calculated between benzimidazole, PA, and water. Second, PT in PA-doped polybenzimidazoles was rigorously modeled at the timescale of picoseconds, using a computationally intensive ab initio molecular dynamics method, atom-centered density matrix propagation (ADMP).[53–59] This was coupled with the ONIOM method[51,52] using density functional theory (DFT) and molecular dynamics (universal force field, UFF[60]) calculations.

## 2. Computational Methodology

### 2.1. Quantum Mechanics Calculations

In order to explore the nature of hydrogen bonding interactions and to compare the energy barriers for different PT pathways in PA-doped polybenzimidazoles, gas-phase properties of several small molecules and ions were investigated using quantum mechanics methods. A benzimidazole molecule, which is the repeat unit structure of poly(2,5-benzimidazole) (ABPBI), was used as the model

for polybenzimidazole. All the quantum mechanics calculations were performed using the B3LYP/6-31 + +G(d,p) level of DFT through the Gaussian 03 program package.[61] The same level of theory and the same version of Gaussian were used to provide the best comparison with our previous quantum mechanics calculations of neat PA.[62]

The proton affinity of the anion ($A^-$) or neutral molecule (B) was calculated as the negative of the enthalpy change based upon a mole of particles for the following reaction:[63]

$$\begin{aligned} A^- + H^+ &\rightarrow HA \\ B + H^+ &\rightarrow BH^+ \end{aligned} \quad (1)$$

The calculated electronic energies of $A^-$ (B) and HA ($BH^+$) at 0 K were corrected with zero-point energy (ZPE)[64] and thermal enthalpies, $H^o$ (298.15 K)–$H^o$ (0 K).[65]

The interaction energy $E_{int}$ between two molecules A and B was calculated as the energy difference between the AB complex and the isolated components A and B, written as:

$$E_{int} = E_{AB} - (E_A + E_B) \quad (2)$$

ZPE corrections[64] and basis set superposition error (BSSE) corrections by the counterpoise approach[66] were also performed to obtain the final corrected interaction energies.

The single coordinate driving (SCD) technique,[67] followed by the quadratic synchronous transit (QST) method (specifically, QST3[68,69]), was utilized to determine energy barriers for different PT pathways between benzimidazole, PA, and water. After fully optimizing the starting geometries using the B3LYP/6-31 + +G(d,p) DFT, SCD with a step size between −0.021 and −0.020 Å was performed along each PT pathway to determine the relative potential energy profile. Due to the hysteresis effect[70] of the SCD technique, the determined energy barriers were also verified by QST3 transition-state optimization.

### 2.2. ADMP Coupled With the ONIOM Scheme

ONIOM[51,52] is a method for combining calculations using high-level calculations on a part of a large system (called the model system), with lower-level calculations on the whole system (called the real system). The ONIOM combination of B3LYP/6-31 + +G(d,p) DFT and UFF[60] can be described by the following expression:[59]

$$E^{ONIOM} = E^{UFF,real} - E^{UFF,model} + E^{ADMP,model} \quad (3)$$

In this case, the real system is treated only by UFF molecular dynamics.[60] Both UFF and B3LYP/6-31 + +G(d,p) DFT are used in the model system. The Gaussian 09 program package[71] was used to perform all the ADMP-ONIOM simulations, where ADMP[53–59] calculations were performed using B3LYP/6-31 + +G(d,p) DFT. To validate the quality of UFF, the bond lengths and angles for water, PA, and ABPBI repeat unit were calculated using UFF, B3LYP/6-31 + +G(d,p) DFT, and the COMPASS force field.[47] Predictions using UFF agree well with DFT and COMPASS. Results are given in Table 1S of the Supporting Information. In the ADMP-ONIOM simulations, polybenzimidazole was represented by five repeat units of ABPBI. Only the repeat unit in the center and all the PA molecules were included in the model system. The coupling quality of polybenzimidazole at the ONIOM (DFT/UFF) interface is also illustrated in the Supporting Information (Figure 1S and Table 2S).

PA-doped polybenzimidazole systems were constructed at three different PA doping levels. In order to make the simulations statistically meaningful, two or three different starting configurations were constructed for each PA doping level and then the geometries were optimized using the ONIOM calculations of B3LYP/6-31 + +G(d,p) DFT and UFF before ADMP-ONIOM simulation. The following three Cases correspond to the three different PA doping levels and each Case includes two or three different configurations: Case 1: two starting configurations were adopted reflecting the two different types of hydrogen bonds, N-H...O=P (Case 1A) and O–H...=N– (Case 1B), between one ABPBI repeat unit and one PA molecule in the model system; Case 2: three different starting configurations were constructed by changing the relative positions of PA molecules to form no hydrogen bond between the two PA molecules (Case 2A), one hydrogen bond between the two PA molecules (Case 2B), and two hydrogen bonds between the two PA molecules (Case 2C) for the model system consisting of one ABPBI repeat unit and two PA molecules; Case 3: three different starting configurations were constructed by varying the relative positions of the three PA molecules for the model system consisting of one benzimidazole moiety and three PA molecules: the three PA molecules constitute roughly a right triangle (Case 3A), the three PA molecules constitute a roughly equilateral triangle (Case 3B), and the three PA molecules are aligned (Case 3C). The relative position of ABPBI and PA molecules for each studied system can be found in the final geometry of each ADMP-ONIOM simulation (Figures 5, 8, and 11).

Electronic embedding was selected to couple the model system and the real system. The unfilled valences in the model system were completed by hydrogen atoms. Each of the ADMP-ONIOM calculations was run for 1 ps using a 0.25-fs time step. Temperature was controlled at 298 K by velocity scaling. The energy profiles of the ADMP-ONIOM simulations for the model system are shown in Figure 2S–9S in the Supporting Information. At the end of each simulation, radial distribution function (RDF) and Fourier transform of the dipole autocorrelation function (FT-DAC) were calculated using the VMD program[72] to study the initial steps of PT and the interfacial properties between PA and polybenzimidazole.

## 3. Results and Discussions

### 3.1. Quantum Mechanics Calculations

#### 3.1.1. Proton Affinity

As listed in Table 1, the calculated proton affinities for the benzimidazole anion and the neutral benzimidazole molecule are 1 419.9 and 951.7 $kJ \cdot mol^{-1}$, respectively. Compared with the proton affinity of PA and water reported in our previous paper,[62] results indicate gas-phase proton affinities ($kJ \cdot mol^{-1}$) in descending order are $O^{2-}$ (2 450.4) > $PO_4^{3-}$ (2 404.4) > $HPO_4^{2-}$ (1 892.5) > $HO^-$ (1 620.2) > benbenzimidazole anion (1 419.9) > $H_2PO_4^-$ (1 359.7) > benzimidazole (951.7) > $H_3PO_4$ (822.6) > $H_2O$ (683.9). Comparing the proton affinities helps to sort these molecules and ions based on their ability to associate a proton in the gas phase. Generally, the larger the proton affinity, the more prone it is to associate a proton, and, therefore, more difficult to dissociate a proton after protonation. As shown, the proton affinity of $H_2PO_4^-$ at 1 359.7 $kJ \cdot mol^{-1}$ is much larger than that of benzimidazole at 951.7 $kJ \cdot mol^{-1}$. This may explain the reason why at lower PA-doping levels, PA forms strong hydrogen bonds with the polybenzimidazole chain, but does not protonate the polymer and forms phosphate itself;[37] however, the solvation effect is not taken into consideration.

#### 3.1.2. Interaction Energy

Table 2 lists the gas-phase interaction energies between benzimidazole, PA, and water molecules, calculated using B3LYP/6-31++G(d,p). Illustrations of these interactions are shown in Figure 1. As indicated in Table 2, there are two types of intermolecular hydrogen bonds between benzimidazole and PA. One is benzimidazole as the hydrogen donor (the "–N(H)–" group) with an interaction energy of −24.7 $kJ \cdot mol^{-1}$ and the other is benzimidazole as the hydrogen acceptor (the "=N–" group) with a much stronger interaction of −45.4 $kJ \cdot mol^{-1}$, which is also stronger than the interaction between two benzimidazole

*Table 1.* Proton affinity values of the benzimidazole, PA, water molecules and their corresponding ions, calculated using B3LYP/6-31++G(d,p).

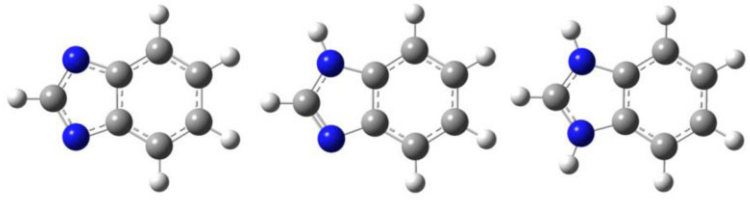

benzimidazole anion  benzimidazole  benzimidazole

| Molecule | $E_{elec}$ [a] | $E_{elec}$ + ZPE [b] | $H$ [c] | Proton affinity [$kJ \cdot mol^{-1}$] [d] |
|---|---|---|---|---|
| benzimidazole anion | −379.3385 | −379.2340 | −379.2273 | 1419.9 |
| benzimidazole | −379.8934 | −379.7752 | −379.7681 | 951.7 |
| benzimidazole cation | −380.2699 | −380.1377 | −380.1306 | – |
| $PO_4^{3-}$ | −641.9813 | −641.9687 | −641.9632 | 2404.4 [e] |
| $HPO_4^{2-}$ | −642.9087 | −642.8846 | −642.8790 | 1892.5 [e] |
| $H_2PO_4^-$ | −643.6431 | −643.6066 | −643.5998 | 1359.7 [e] |
| $H_3PO_4$ | −644.1732 | −644.1250 | −644.1177 | 822.6 [e] |
| $H_4PO_4^+$ | −644.4977 | −644.4383 | −644.4310 | – |
| $O^{2-}$ | −74.8610 | −74.8610 | −74.8587 | 2450.4 [e] |
| $HO^-$ | −75.8038 | −75.7953 | −75.7920 | 1620.2 [e] |
| $H_2O$ | −76.4341 | −76.4129 | −76.4091 | 683.9 [e] |
| $H_3O^+$ | −76.7062 | −76.6734 | −76.6696 | – |

[a] Electronic energy $E_{elec}$ in Hartrees; [b] Electronic energy with ZPE correction in Hartrees; [c] Sum of electronic energy and thermal enthalpy correction, $H^o$ (298.15 K) − $H^o$ (0 K), in Hartrees; [d] 1 Hartree = 2625.5 $kJ \cdot mol^{-1}$; [e] Calculated proton affinity for PA and water species in ref.[62]

*Table 2.* Interaction energies $E_{int}$ between benzimidazole, PA, and water, calculated using B3LYP/6-31++G(d,p).

| | $E_{elec}$ [a)] | $E_{elec} + ZPE$ [b)] | $E_{elec} + ZPE + BSSE$ [c)] | $E_{int}$ [kJ · mol$^{-1}$] [d)] |
|---|---|---|---|---|
| Benzimidazole | −379.8934 | −379.7752 | – | – |
| PA | −644.1732 | −644.1249 | – | – |
| Water | −76.4341 | −76.4129 | – | – |
| Benzimidazole · benzimidazole | −759.8006 | −759.5627 | −759.5619 | −30.2 |
| Benzimidazole · PA (1) | −1024.0780 | −1023.9105 | −1023.9095 | −24.7 |
| Benzimidazole · PA (2) | −1024.0875 | −1023.9191 | −1023.9174 | −45.4 |
| Benzimidazole · water (1) | −456.3383 | −456.1969 | −456.1954 | −19.2 |
| Benzimidazole · water (2) | −456.3391 | −456.1967 | −456.1958 | −20.2 |
| PA · PA [e)] | −1288.3832 | −1288.2848 | −1288.2821 | −84.8 [f)] |
| PA · water [e)] | −720.6279 | −720.55418 | −720.5524 | −38.3 [f)] |
| Water · water | −152.8777 | −152.8318 | −152.8306 | −12.6 [f)] |

[a)]Total electronic energy in Hartrees; [b)]Total electronic energy corrected for ZPE in Hartrees; [c)]Total electronic energy corrected for both ZPE and BSSE in Hartrees; [d)]1 Hartree = 2 625.5 kJ · mol$^{-1}$; [e)]Two intermolecular hydrogen bonds co-exist in each molecule pair; [f)]Calculated interaction energy between water and PA in ref.[62]

molecules (−30.2 kJ · mol$^{-1}$). These interaction energy differences may suggest the hydrogen bond with benzimidazole as a hydrogen acceptor is the major interaction between polybenzimidazole and PA molecules at low PA-doping levels. The strong hydrogen bond between PA and the "=N–" group on the imidazole ring has also been confirmed by infrared spectroscopy.[39,40]

Similarly, there are two types of hydrogen bonds between benzimidazole and water. The interaction energy for the one with benzimidazole as hydrogen donor is −19.2 kJ · mol$^{-1}$; the other with water as hydrogen donor has a similar interaction energy of −20.2 kJ · mol$^{-1}$. This suggests near equal possibilities for both to form hydrogen bonds in the gas phase. These results agree with the hydrogen bond network model proposed by Brooks et al.[44] for hydrated PBI. Brooks et al. measured the water uptake of polybenzimidazoles and concluded that hydrogen bonding in hydrated PBI occur in two ways as the interaction energies suggest.

The calculated interaction energy values for the PA…PA pair and the PA… water pair are −84.8 and −38.3 kJ · mol$^{-1}$, respectively.[62] The relatively stronger interactions for both the PA···PA pair and the PA···water pair include contributions from two intermolecular hydrogen bonds, as illustrated in Figure 1. The water…water interaction is the weakest among all pairs, at −12.6 kJ · mol$^{-1}$.[62] From these results, it can be concluded that the strength of interaction (kJ · mol$^{-1}$) between any two of the three molecules range in descending order as follows: PA···PA (–84.8*)[62] > PA (H-donor)···benzimidazole (–45.4) > PA···water (–38.3*)[62] > benzimidazole···benzimidazole (–30.2) > benzimidazole (H-donor)···PA (–24.7) > water (H-donor)···benzimidazole (–20.2), benzimidazole (H-donor)···water (–19.2) > water···water (–12.6),[62] where the asterisk (*) denotes contributions coming from two intermolecular hydrogen bonds. A more negative energy value indicates a stronger interaction.

### 3.1.3. Energy Barriers for Different PT Pathways

The relative energy profiles for different PT pathways obtained by the SCD technique accompanied by corresponding starting and final geometries are shown in Figure 2–4. Directions of the PT are indicated by arrows in both relative energy profiles and starting geometries. The relative energy profiles for PT between PA, water, and their corresponding ions can be found in our previous publication.[62]

Figure 2 shows results of PT between benzimidazole and benzimidazole/benzimidazole ions. Specifically, PT from benzimidazole cation to benzimidazole (Case 1), PT between two benzimidazole molecules (Case 2), and PT from benzimidazole to benzimidazole anion (Case 3) were studied. As shown, the energy barrier for PT from a benzimidazole cation to a neutral benzimidazole molecule (Case 1) is 4.1 kJ · mol$^{-1}$ at the $^{13}$N–$^{14}$H···$^{30}$N distance of 1.28 Å, which is the smallest energy barrier among the three PT pathways. The relative energy profile for PT between two neutral benzimidazole molecules (Case 2) is monotonically increasing along the proposed PT direction and the final energy barrier is about 113.9 kJ · mol$^{-1}$ at the $^{29}$N-$^{27}$H···$^{14}$N distance of 1.04 Å. The energy barrier for PT from a neutral benzimidazole molecule to an anion (Case 3)

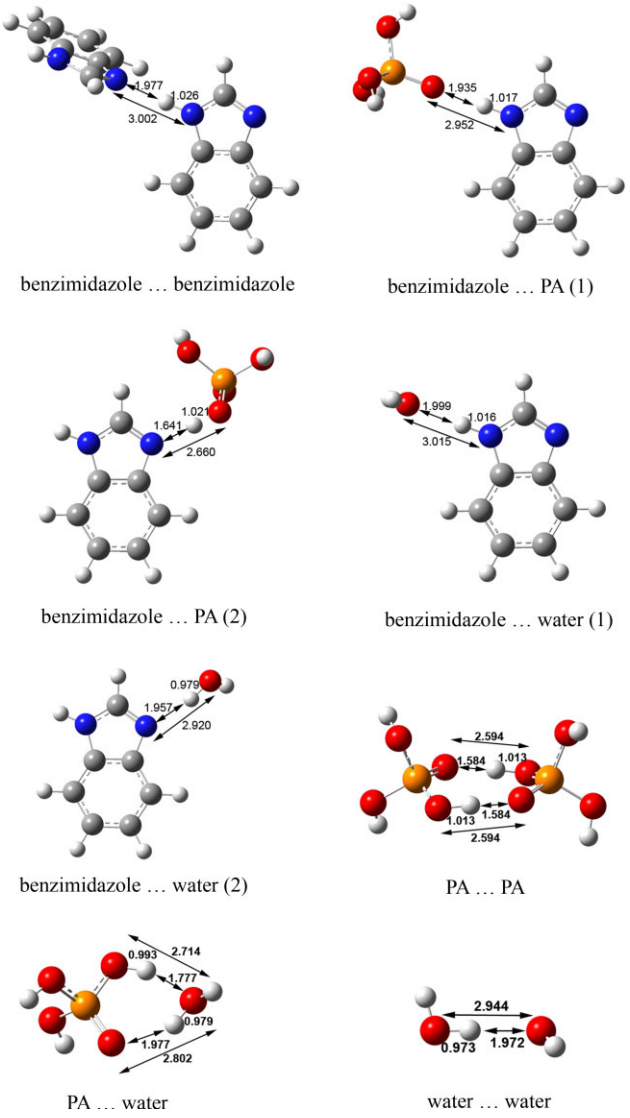


*Figure 1.* Illustration of the interactions between benzimidazole, PA, and water, calculated using B3LYP/6-31++G(d,p).

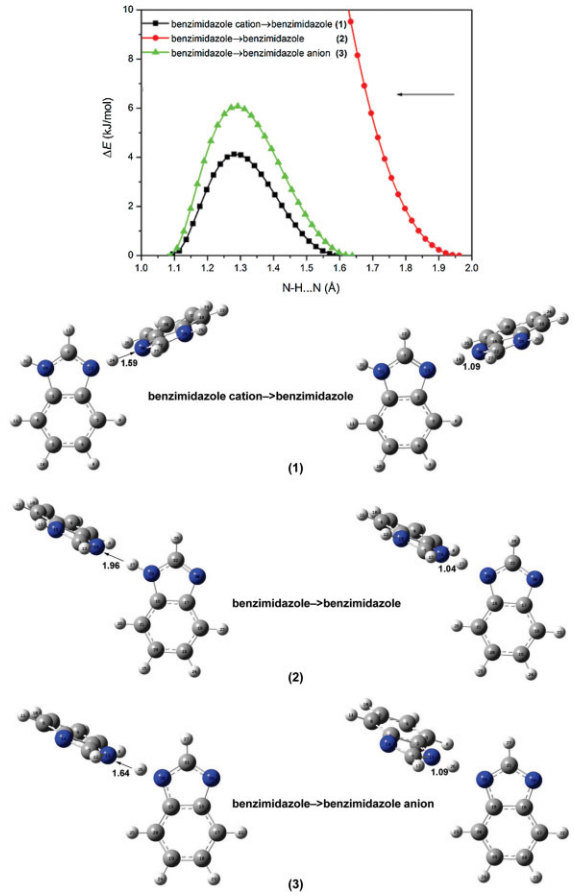


*Figure 2.* Relative energy profile for PT between benzimidazole and benzimidazole/benzimidazole ions, obtained from SCD calculations using B3LYP/6-31++G(d,p) DFT, followed by the corresponding starting and final geometries illustrated on the left and right, respectively (arrows indicate the PT direction) (1) benzimidazole cation → benzimidazole; (2) benzimidazole → benzimidazole; (3) benzimidazole → benzimidazole anion.

is 6.1 kJ · mol$^{-1}$ at the $^{28}$N–$^{26}$H···$^{13}$N distance of 1.29 Å, a little larger than the energy barrier of PT from a cation to a neutral molecule. This is consistent with the proton affinity results that the proton affinity of the benzimidazole anion (1 419.9 kJ · mol$^{-1}$) is larger than that of the neutral benzimidazole (951.7 kJ · mol$^{-1}$).

Figure 3 shows results of PT between benzimidazole and PA/phosphate ions. For the pair of benzimidazole and the phosphate cation ($H_4PO_4^+$), the excess proton moves to the benzimidazole molecule after the initial optimization. This agrees with the proton affinity results that the proton affinity of benzimidazole (951.7 kJ · mol$^{-1}$) is larger than that of PA (822.6 kJ · mol$^{-1}$),[62] suggesting an absence of energy barrier for PT. The calculated relative energy profiles include PT from benzimidazole cation to PA (Case 1), PT from benzimidazole to PA (Case 2), PT from PA to benzimidazole (Case 3), and PT from benzimidazole to phosphate anion ($H_4PO_4^-$) (Case 4). All the relative energy profiles presented in this figure are monotonically increasing (from right to left). The energy barrier for PT from benzimidazole cation to PA (Case 1) was calculated to be 69.6 kJ · mol$^{-1}$, larger than the energy barrier of PT from benzimidazole to phosphate anion (Case 4), which is 36.5 kJ · mol$^{-1}$. This is also consistent with the previous proton affinity results that the proton affinity difference between benzimidazole (951.7 kJ · mol$^{-1}$) and $H_3PO_4$ (822.6 kJ · mol$^{-1}$)[62] is greater than that between benzimidazole anion (1 419.9 kJ · mol$^{-1}$) and $H_4PO_4^-$ (1 359.7 kJ · mol$^{-1}$).[62] The curve for PT from benzimidazole to PA (Case 2) breaks when the $^{13}$N–$^{14}$H···$^{23}$O distance decreases below 1.6 Å due to a too high energy barrier. The PT from PA to benzimidazole (Case 3) also shows a high energy barrier of ≈114.4 kJ · mol$^{-1}$.

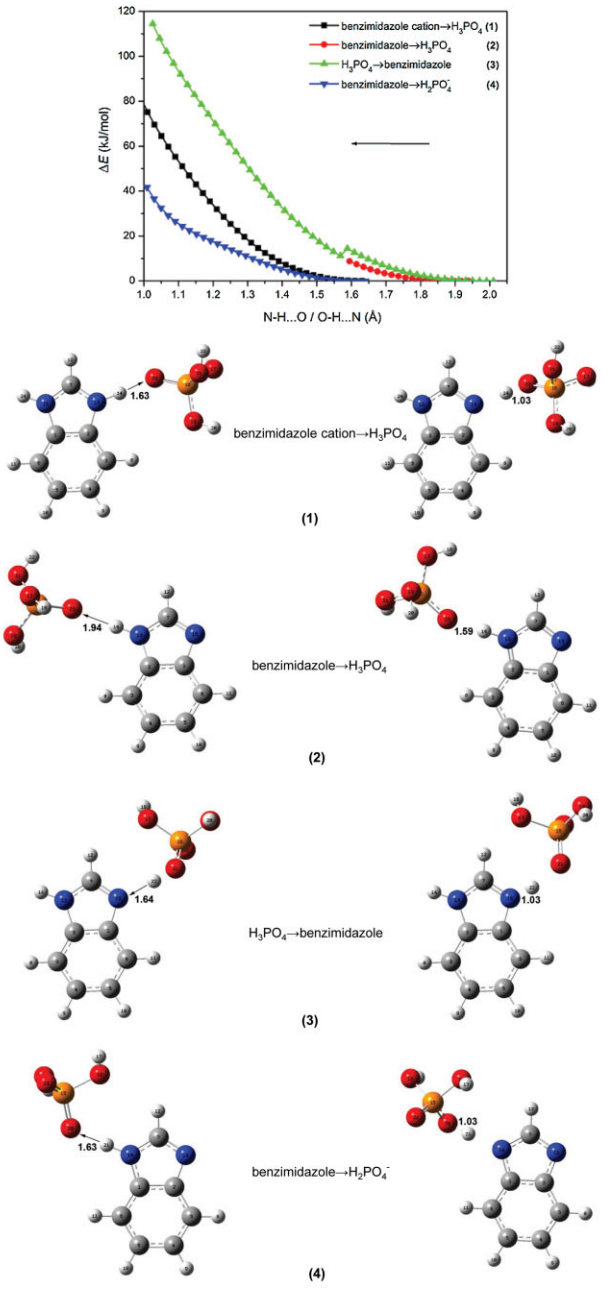


*Figure 3.* Relative energy profile for PT between benzimidazole and PA/phosphate ions, obtained from SCD calculations using B3LYP/6-31++G(d,p) DFT, followed by the corresponding starting and final geometries illustrated on the left and right, respectively (arrows indicate the PT direction) (1) benzimidazole cation → $H_3PO_4$; (2) benzimidazole → $H_3PO_4$; (3) $H_3PO_4$ → benzimidazole; (4) benzimidazole → $H_2PO_4^-$.

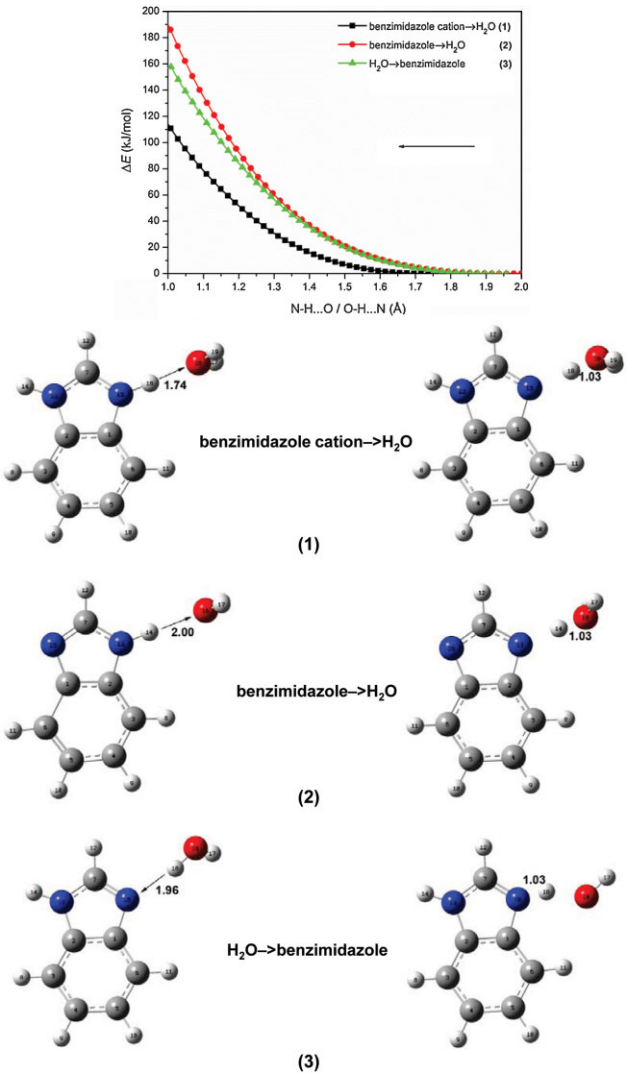


*Figure 4.* Relative energy profile for PT between benzimidazole and water/hydronium ion, obtained from SCD calculations using B3LYP/6-31++G(d,p) DFT, followed by the corresponding starting and final geometries illustrated on the left and right, respectively (arrows indicate the PT direction) (1) benzimidazole cation → $H_2O$; (2) benzimidazole → $H_2O$; (3) $H_2O$ → benzimidazole.

Figure 4 shows results of PT between benzimidazole and water/hydronium ion. Similar to Figure 3, all the relative energy profiles presented in Figure 4 are monotonically increasing (from right to left) and, for the pair of benzimidazole and hydronium ion ($H_3O^+$), the excess proton moves to benzimidazole after the initial optimization due to the higher proton affinity of benzimidazole (951.7 kJ · mol$^{-1}$) compared to that of water (683.9 kJ · mol$^{-1}$).[62] The relative energy profile in Figure 4 includes three curves for PT from benzimidazole cation to water (Case 1), PT from benzimidazole to water (Case 2), and PT from water to benzimidazole (Case 3), respectively. The energy barrier for PT from benzimidazole cation to water was calculated to be 102.7 kJ · mol$^{-1}$. The energy barriers for PT from benzimidazole to water and from water to benzimidazole are 173.5 and 148.1 kJ · mol$^{-1}$, respectively.

Table 3 summarizes the energy barriers for different PT pathways and the corresponding N(O)–H···N(O) distances

*Table 3.* Energy barriers for different PT pathways and their corresponding N(O)-H ··· N(O) distances, predicted by the SCD method and QST3 optimization, both using B3LYP/6-31++G(d,p).

| PT pathways | SCD | | QST3 | | Ref. |
|---|---|---|---|---|---|
| | N(O)-HN(O) distance [Å] | Energy barrier [kJ/mol] | N(O)-HN(O) distance [Å] | Energy barrier [kJ/mol] | |
| benzimidazole cation → benzimidazole (1) | 1.28 | 4.1 | 1.286[a)] | 4.1 | Fig. 2 |
| benzimidazole → benzimidazole (2) | 1.04 | 113.9 | — | — | |
| benzimidazole → benzimidazole anion (3) | 1.29 | 6.1 | 1.288[b)] | 6.1 | |
| benzimidazole cation → $H_3PO_4$ (1) | 1.03 | 69.6 | — | — | Fig. 3 |
| benzimidazole → $H_3PO_4$ (2) | break | break | — | — | |
| $H_3PO_4$ → benzimidazole (3) | 1.03 | 114.4 | — | — | |
| benzimidazole → $H_2PO_4^-$ (4) | 1.03 | 36.5 | — | — | |
| benzimidazole cation → $H_2O$ (1) | 1.03 | 102.7 | — | — | Fig. 4 |
| benzimidazole → $H_2O$ (2) | 1.03 | 173.5 | — | — | |
| $H_2O$ → benzimidazole (3) | 1.03 | 148.1 | — | — | |
| $H_4PO_4^+$ → $H_3PO_4$ | 1.03 | 4.9 | — | — | Ref. [62] |
| $H_3PO_4$ → $H_3PO_4$ | 1.19 | 16.0 | 1.199[c)] | 16.0 | |
| $H_3PO_4$ → $H_2PO_4^-$ | 1.21 | 5.4 | 1.211[d)] | 5.3 | |
| $H_4PO_4^+$ → $H_2O$ | 1.03 | 29.5 | — | — | Ref. [62] |
| $H_3PO_4$ → $H_2O$ | 1.13 | 47.2 | 1.135[e)] | 47.1 | |

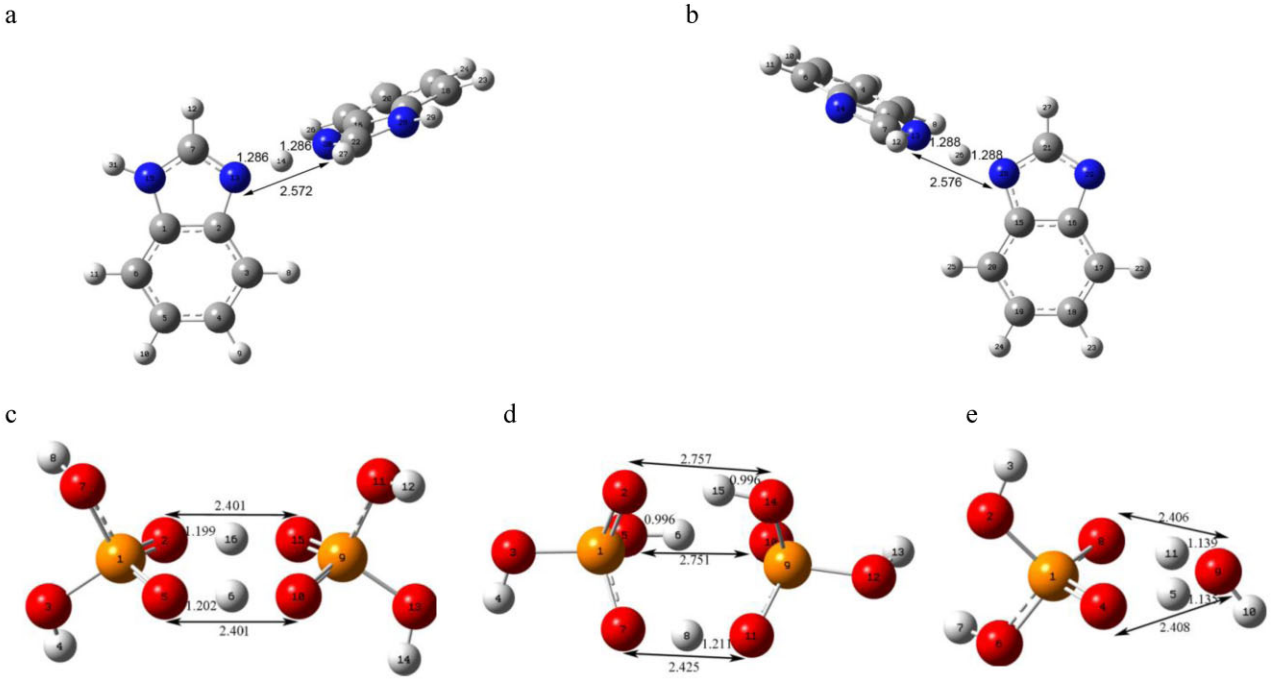

determined by SCD and QST3 methods, respectively. The optimized transition state structures using the QST3 method are also summarized in Table 3 when the transition state exists. Results indicate that the SCD outcomes agree well with those from QST3, which means the hysteresis effect of the SCD method is not significant in this case. Generally, the lower the energy barrier, the easier PT can occur. Three no-barrier PTs including "$H_3O^+ \rightarrow H_3PO_4$", "$H_3O^+ \rightarrow$ benzimidazole", and "$H_4PO_4^+ \rightarrow$ benzimidazole" were observed in the SCD calculations. Except for the three no-barrier PT pathways, PT occurring between the same molecules or between a molecule and its corresponding ion generally shows a smaller energy barrier than PT occurring between different molecular/ionic species. Specifically, the energy barriers ($kJ \cdot mol^{-1}$) for different PT pathways in ascending order are: "benzimidazole cation $\rightarrow$ benzimidazole (4.1)" < "$H_4PO_4^+ \rightarrow H_3PO_4$ (4.9)" < $H_3PO_4 \rightarrow H_2PO_4^-$ (5.4)' < "benzimidazole $\rightarrow$ benzimidazole anion (6.1)" < "$H_3PO_4 \rightarrow H_3PO_4$ (16.0)" < "$H_4PO_4^+ \rightarrow H_2O$ (29.5)" < "benzimidazole $\rightarrow H_2PO_4^-$ (36.5)" < "$H_3PO_4 \rightarrow H_2O$ $H_2O$ (47.2)" < "benzimidazole cation $\rightarrow H_3PO_4$ (69.6)" "benzimidazole cation $\rightarrow H_2O$ (102.7)" < "benzimidazole $\rightarrow$ benzimidazole (113.9)", "$H_3PO_4 \rightarrow$ benzimidazole (114.4)" < "benzimidazole $\rightarrow H_3PO_4$", "$H_2O \rightarrow$ benzimidazole (148.1)" < "benzimidazole $\rightarrow H_2O$ (173.5)". It is worth mentioning the calculated energy barriers are for protons transferring between two molecules or between a molecule and an ion in the gas state. In the liquid phase, there are generally multiple protons continuously hopping along a cluster of molecules and ions, which decreases the calculated energy barrier and can potentially enable PT along the pathways associated with high energy barriers as well.

### 3.2. ADMP-ONIOM Simulations on PA-Doped ABPBI

Experimental infrared spectra of neat ABPBI [29] indicate a free N–H, hydrogen-bonded N···H, and water O–H stretching vibrations explicitly between 3 000 to 3 600 $cm^{-1}$, whereas the PA-doped ABPBI shows a broad peak from 2 500 to 3 500 $cm^{-1}$ describing a strong hydrogen bond network. In PA-doped ABPBI, a general protonated $N^+$–H stretching at ≈2 800 $cm^{-1}$ also replaces explicit vibration modes for neat ABPBI.[29,73] In this part of study, FT-DACs were calculated from the 1-ps ADMP-ONIOM simulation trajectory to compare with the experimental infrared spectra. Meanwhile, RDFs were also calculated to investigate the interfacial properties between PA and polybenzimidazole.

#### 3.2.1. Case 1: Model System of 1 ABPBI Repeat Unit and 1 PA Molecule

Figure 5 shows the final geometries at the end of the 1-ps ADMP-ONIOM simulation from two different starting configurations for the model system consisting of one ABPBI repeat unit and one PA molecule. The two configurations correspond to two types of hydrogen bonds, "N–H···O=P" for the configuration of Case 1A and "O–H···=N–" for the configuration of Case 1B. As shown, no protonation ($N^+$–H) occurred during the simulations for either of the two configurations.

Figure 6 shows the calculated FT-DACs for the 1-ps ADMP-ONIOM simulations from both starting configurations. Because both simulated systems contain only one hydrogen bond between a benzimidazole moiety and a PA molecule, Figure 6 does not show a broad peak around 3 000 $cm^{-1}$. But it still qualitatively denotes N–H and O–H stretching above 3 000 $cm^{-1}$, P–O stretching and bending around 1 000 $cm^{-1}$, and O–H and N–H bending around 500 $cm^{-1}$ for both configurations. The small peaks between 1 000 and 2 000 $cm^{-1}$ respond to the phenyl and imidazole rings.

Figure 7 shows the calculated RDFs for the N···H and N···O atom pairs during the 1-ps ADMP-ONIOM runs from two different starting configurations. In Case 1A,

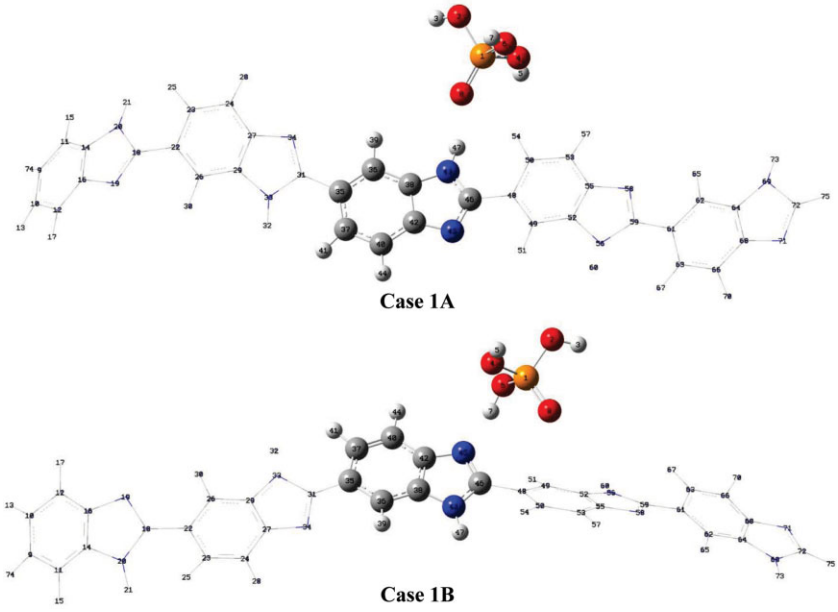


*Figure 5.* The final geometries at the end of the 1-ps ADMP-ONIOM simulations from two different starting configurations for the model system consisting of one ABPBI repeat unit and one PA molecule.

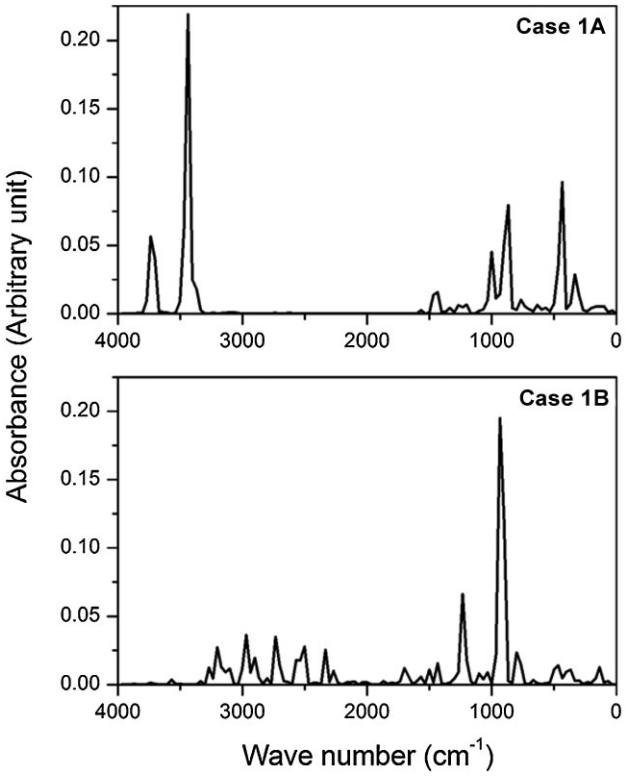


*Figure 6.* Calculated FT-DACs for the 1-ps ADMP-ONIOM runs from two different starting configurations for the model system consisting of one ABPBI repeat unit and one PA molecule.

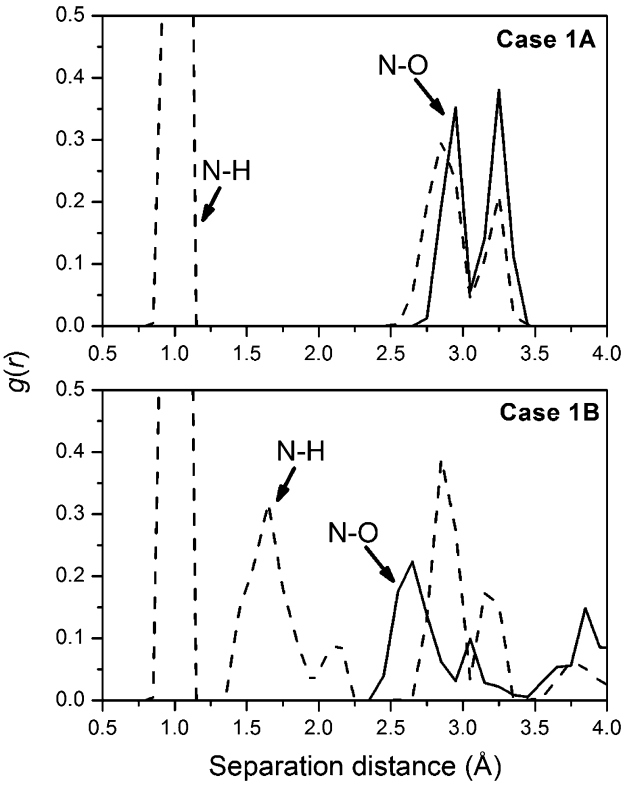


*Figure 7.* Calculated RDFs for the N···H and N···O atom pairs during the 1-ps ADMP-ONIOM runs from two different starting configurations for the model system consisting of one ABPBI repeat unit and one PA molecule.

the hydrogen bond is in the form of "N–H···O=P". RDF for the N···H atom pair, $g_{N-H}(r)$, shows the first peak at 1 Å corresponding to the N–H covalent bond, RDF for the N–O atom pair, $g_{N-O}(r)$, shows two peaks at 2.9 and 3.2 Å reflecting a fluctuating distance between hydrogen donor and acceptor. In Case 1B, the hydrogen bond is in the form of "O–H···=N–". Besides the first peak at 1 Å denoting the N–H covalent bond, RDF for the N···H atom pair, $g_{N-H}(r)$, shows a second peak at 1.6 Å corresponding to the hydrogen bond length. RDF for the N···O atom pair, $g_{N-O}(r)$, shows the distance between hydrogen donor and acceptor at 2.6 Å. These results agree well with MD simulation results using the COMPASS force field.[47]

### 3.2.2. Case 2: Model System of 1 ABPBI Repeat Unit and 2 PA Molecules

Figure 8 shows the final geometries at the end of the 1-ps ADMP-ONIOM runs from three different starting configurations for the model system consisting of one ABPBI repeat unit and two PA molecules. As previously introduced, the three configurations correspond to three different positions of the two PA molecules: (Case 2A) no hydrogen bond between the two PA molecules; (Case 2B) one hydrogen bond between the two PA molecules; and (Case 2C) two hydrogen bonds between the two PA molecules. It can be seen that the protonation ($N^+$–H) occurs only in the configuration of Case 2C where two hydrogen bonds are formed between the two PA molecules.

Figure 9 shows the calculated FT-DACs for 1-ps ADMP-ONIOM runs from the three different starting configurations. As expected, the peaks around 3 000 $cm^{-1}$ get broader indicating more hydrogen bonds as the increases of PA doping levels. The broadest peak in Case 2C corresponds to the protonation ($N^+$–H), which agrees well with the experimental infrared spectra of PA-doped ABPBI.[29,73]

Figure 10 shows the calculated RDFs for the O···H and O···O atom pairs for the corresponding 1-ps ADMP runs from the three different starting configurations. Comparing RDFs for the N···H atom pair, $g_{N-H}(r)$, in the three configurations, it can be seen that the second peak at around 1.7 Å disappears in Case 2C. This is solid evidence for the occurrence of protonation ($N^+$–H). In addition, the corresponding distance between N and O atoms also decreases to 2.5 Å as the protonation occurs.

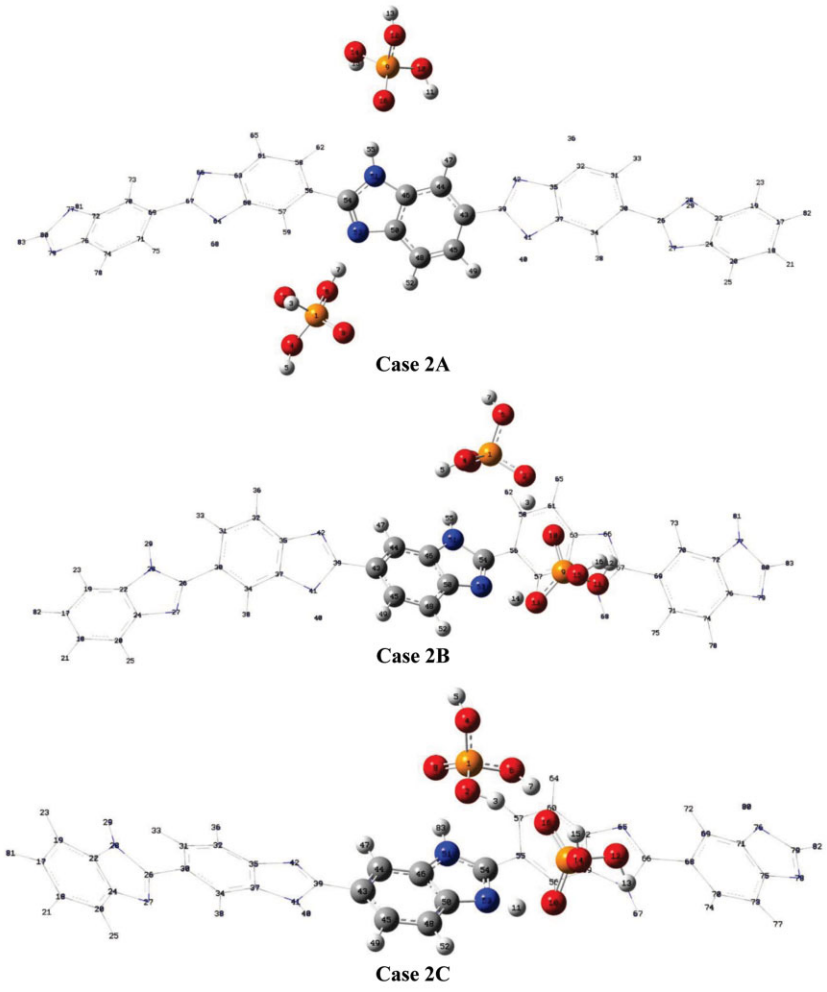


*Figure 8.* The final geometries at the end of the 1-ps ADMP-ONIOM simulations from three different starting configurations for the model system consisting of one ABPBI repeat unit and two PA molecules.

### 3.2.3. Case 3: Model System of 1 ABPBI Repeat Unit and 3 PA Molecules

Figure 11 shows the final geometries at the end of the 1-ps ADMP-ONIOM runs from three different starting configurations for the model system consisting of one ABPBI repeat unit and three PA molecules. In this case, the three configurations correspond to three different relative positions of the three PA molecules: (Case 3A) the three PA molecules constitute a roughly right triangle; (Case 3B) the three PA molecules constitute a roughly equilateral triangle; and (Case 3C) the three PA molecules are aligned. It can be seen that protonation ($N^+$–H) occurs in the configurations of Case 3B and Case 3C, where a third PA molecule forms multiple hydrogen bonds with both of the two PA molecules that form hydrogen bonds with the benzimidazole moiety. While in Case 3A, only one hydrogen bond exists between the two PA molecules that form hydrogen bonds with the benzimidazole moiety and the third PA molecule form hydrogen bonds with only one PA. In addition, Figure 11 shows a larger deformation of the ABPBI chain compared to Figures 5 and 8, indicating a stronger coupling between the polymer chain and PA molecules as more PA molecules are added.

Figure 12 shows the calculated FT-DACs for 1-ps ADMP-ONIOM runs from the three different starting configurations. Results show broader peaks around 3 000 $cm^{-1}$ in the configurations of Case 3B and Case 3C, denoting the protonation ($N^+$–H), which also agrees with the experimental infrared spectra of PA-doped ABPBI.[29,73]

Figure 13 shows the calculated RDFs for the O···H and O···O atom pairs for the corresponding 1-ps ADMP runs from the three different starting configurations. Comparing

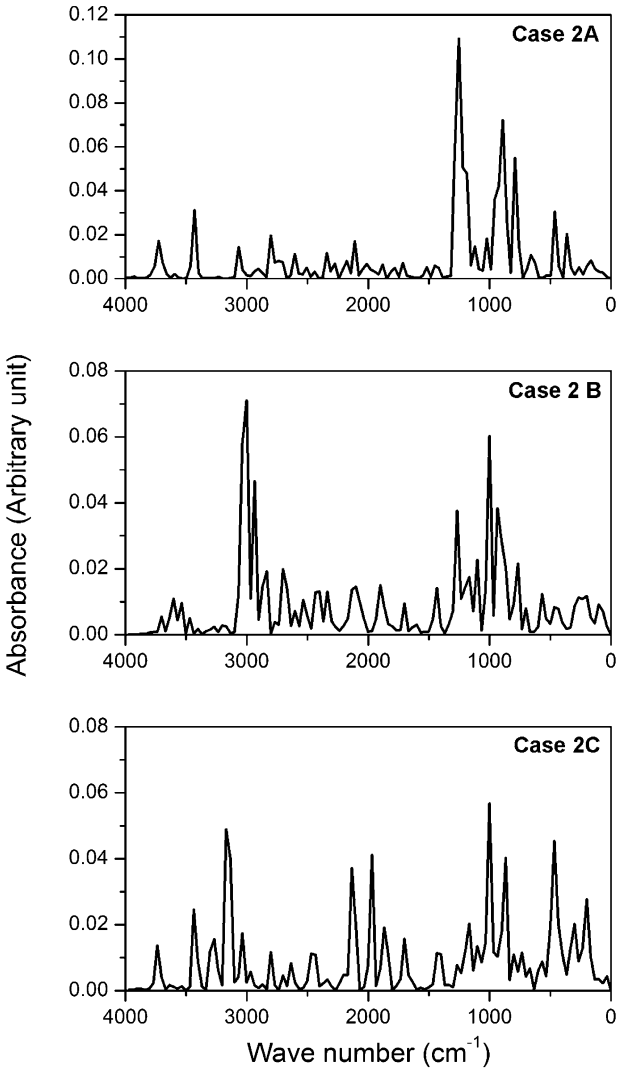


*Figure 9.* Calculated FT-DACs for the 1-ps ADMP-ONIOM runs from three different starting configurations for the model system consisting of one ABPBI repeat unit and two PA molecules.

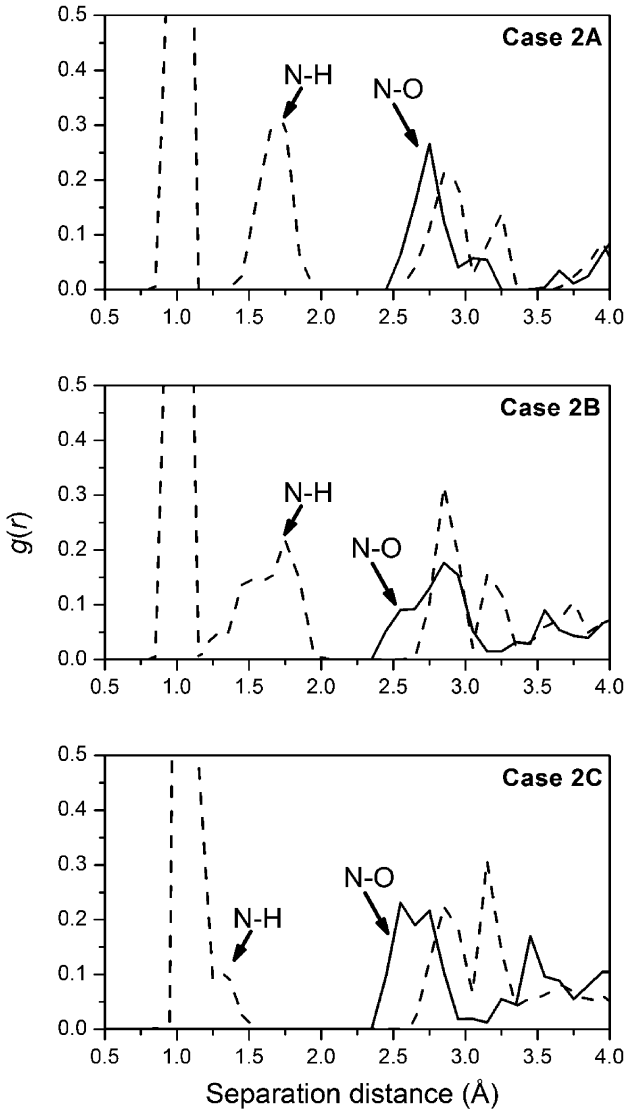


*Figure 10.* Calculated RDFs for the N···H and N···O atom pairs during the 1-ps ADMP-ONIOM runs from three different starting configurations for the model system consisting of one ABPBI repeat unit and two PA molecules.

RDFs for the N···H atom pair, $g_{N-H}(r)$, in the three configurations, it can be seen that only Case 3A shows an obvious second peak at ≈1.6 Å, corresponding to the hydrogen bonding. In Case 3B this peak gets very small and in Case 3C the peak disappears, providing solid evidence for the occurrence of protonation ($N^+$–H).

## 4. Conclusion

In this study, quantum mechanics calculations using B3LYP/6-31++G(d,p) DFT were performed to calculate gas-phase proton affinity, interaction energy, and energy barriers for different PT pathways between the benzimidazole, PA, water molecules and their corresponding ions. The gas-phase proton affinity results indicate a larger proton affinity of $H_2PO_4^-$ (1 359.7 kJ · mol$^{-1}$) compared to benzimidazole (951.7 kJ · mol$^{-1}$). This explains the reason why PA forms strong hydrogen bond with the polybenzimidazole chain but does not protonate the polymer and forms phosphate itself at lower PA-doping levels. The stronger interaction of "PA (H-donor)···benzimidazole (–45.4 kJ · mol$^{-1}$)" compared to "benzimidazole···benzimidazole (–30.2 kJ · mol$^{-1}$)" and "benzimidazole (H-donor)···PA (–24.7 kJ · mol$^{-1}$)" suggests the hydrogen bond of "PA (H-donor)···benzimidazole" is the major interaction

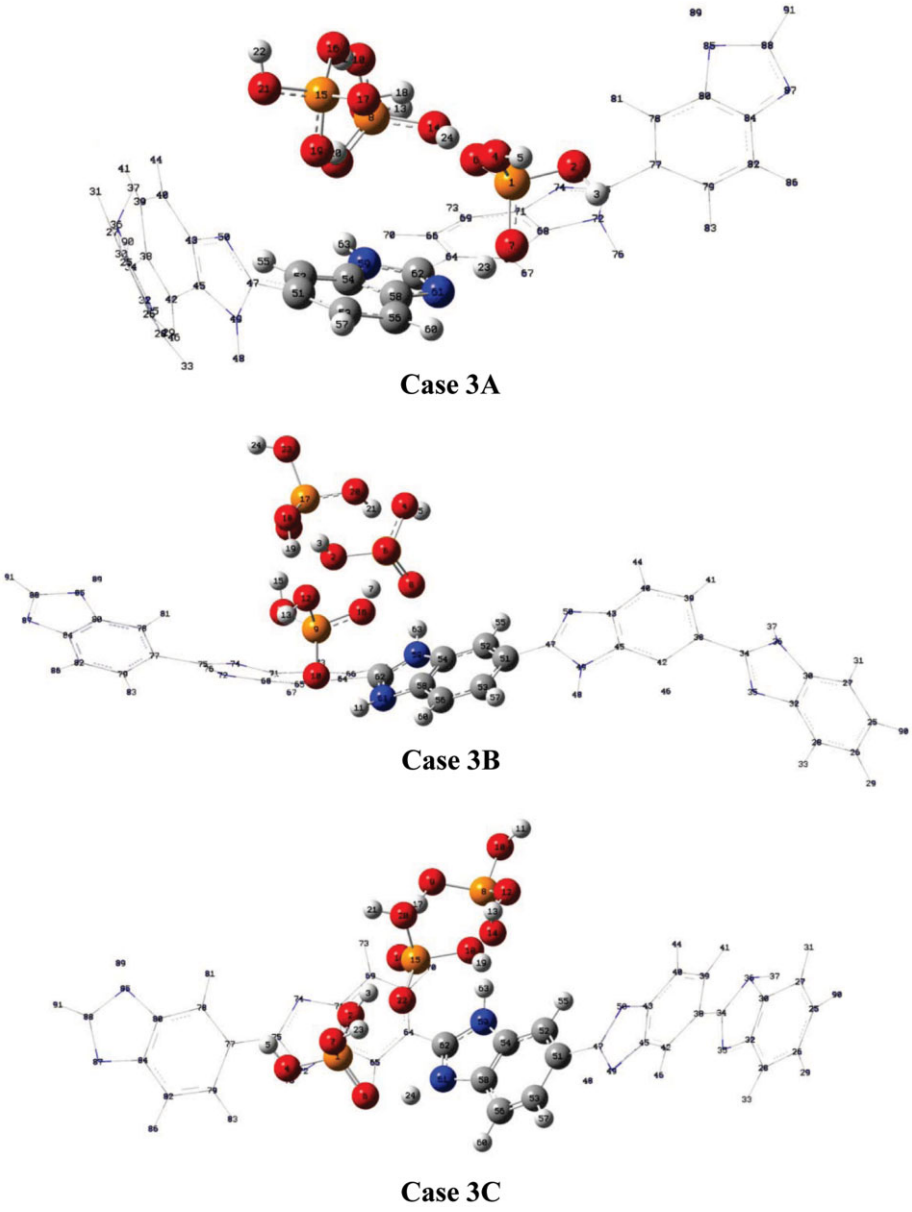


*Figure 11.* The final geometries at the end of the 1-ps ADMP-ONIOM Simulations from three different starting configurations for the model system consisting of one ABPBI repeat unit and three PA molecules.

pattern between polybenzimidazole and PA molecules at low PA-doping levels. While for interactions between polybenzimidazole and water molecules, similar interaction energies of "water (H-donor)···benzimidazole ($-20.2\ kJ \cdot mol^{-1}$)" and "benzimidazole (H-donor)···water ($-19.2\ kJ \cdot mol^{-1}$)" suggest near equal possibilities to form both hydrogen bonds in the hydrated polybenzimidazole. The determined energy barriers for different PT pathways indicate that PT occurring between the same molecules or between a molecule and its corresponding ion generally is more prone to occur compared to PT occurring between different molecular/ionic species.

ADMP coupled with the ONIOM (DFT/UFF) scheme was used to study the initial steps of PT in the PA-doped ABPBI system and the interfacial properties between ABPBI and PA. Results indicate that protonation of the "$=N-$" atom on the imidazole ring of ABPBI occurs when there are two or more PA molecules surrounding each ABPBI repeat unit, which agrees with the experimental results.[37] In addition, this simulation study explains how protonation ($N^{+}-H$) occurs. When there are two PA molecules per ABPBI repeat unit in the system, protonation occurs only when two hydrogen bonds exist between the two PA molecules that are hydrogen-bonded to the imidazole ring. When there are

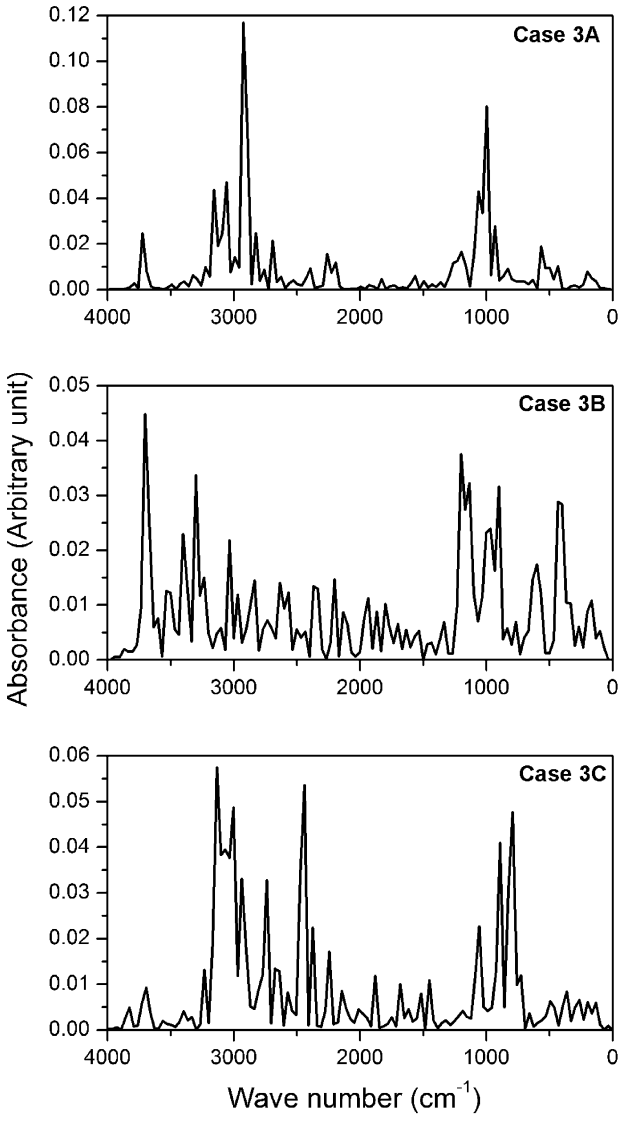


*Figure 12.* Calculated FT-DACs for the 1-ps ADMP-ONIOM runs from three different starting configurations for the model system consisting of one ABPBI repeat unit and three PA molecules.

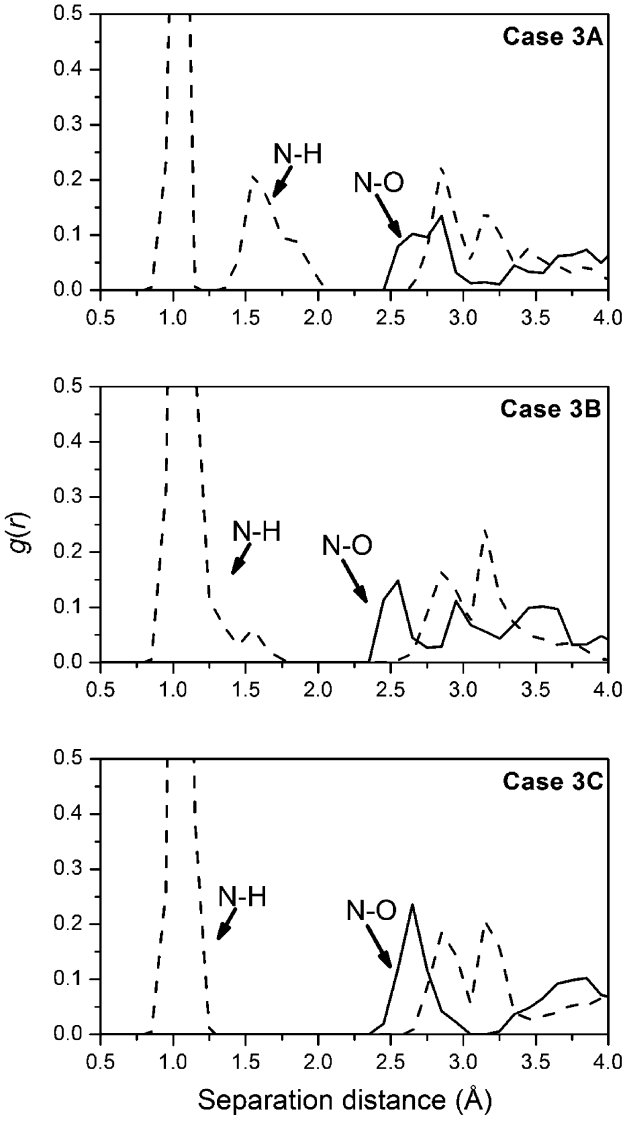


*Figure 13.* Calculated RDFs for the N···H and N···O atom pairs during the 1-ps ADMP-ONIOM runs from three different starting configurations for the model system consisting of ABPBI repeat unit and three PA molecules.

three PA molecules per ABPBI repeat unit in the system, the two PA molecules that are hydrogen-bonded to the imidazole ring can have only one hydrogen bond or even no hydrogen bond, but a third PA molecule has to form hydrogen bonds with both of the two PA molecules in order to protonate the "=N–" atom. The occurrence of protonation has also been verified by the disappearance of the RDF peak for the "O–H···=N–" hydrogen bond. Calculated FT-DACs agree reasonably well with the experimental infrared spectra. An attempt to investigate the effect of an excess water molecule on the PT mechanism in PA-doped ABPBI was unsuccessfully due to using a too small model system, which underestimated the solvation effect[74,75] for the water molecule.

Acknowledgements: Acknowledgement is made to the donors of the American Chemical Society Petroleum Research Fund (ACS PRF # 45666-AC5) for financial support. This work was also supported by an allocation of computing time from the Ohio Supercomputer Center.

Received: January 7, 2013; Revised: March 29, 2013; Published online: July 19, 2013; DOI: 10.1002/mats.201300002

Keywords: ab initio molecular dynamics; fuel cells; ONIOM; proton transfer; quantum chemistry

[1] N. Agmon, *Chem. Phys. Lett.* **1995**, *244*, 456.
[2] R. Devanathan, A. Venkatnathan, R. Rousseau, M. Dupuis, T. Frigato, W. Gu, V. Helms, *J. Phys. Chem. B.* **2010**, *114*, 13681.

[3] K. D. Kreuer, S. J. Paddison, E. Spohr, M. Schuster, *Chem. Rev.* **2004**, *104*, 4637.
[4] S. S. Iyengar, C. J. Burnham, M. K. Petersen, G. A. Voth, *Comput. Sci. Eng.* **2003**, *5*, 31.
[5] US.3718627 (1968), E.I. du Pont de Nemours and invs.: W. G. Grot,
[6] R. Devanathan, *Energy Environ. Sci.* **2008**, *1*, 101.
[7] M. Eikerling, S. J. Paddison, L. R. Pratt, T. A. Zawodzinski, *Chem. Phys. Lett.* **2003**, *368*, 108.
[8] S. J. Paddison, J. A. Elliott, *J. Phys. Chem. A.* **2005**, *109*, 7583.
[9] S. J. Paddison, J. A. Elliott, *Solid State Ionics.* **2007**, *178*, 561.
[10] A. Roudgar, S. P. Narasimachary, M. Eikerling, *J. Phys. Chem. B.* **2006**, *110*, 20469.
[11] A. Roudgar, S. P. Narasimachary, M. Eikerling, *Chem. Phys. Lett.* **2008**, *457*, 337.
[12] Y. Choe, E. Tsuchida, T. Ikeshoji, S. Yamakawa, S. Hyodo, *Phys. Chem. Chem. Phys.* **2009**, *11*, 3892.
[13] G. A. Luduena, T. D. Kuehne, D. Sebastiani, *Chem. Mat.* **2011**, *23*, 1424.
[14] S. Ahadian, H. Mizuseki, Y. Kawazoe, *J. Membr. Sci.* **2011**, *369*, 339.
[15] V. A. Glezakou, M. Dupuis, C. J. Mundy, *Phys. Chem. Chem. Phys.* **2007**, *9*, 5752.
[16] E. Spohr, P. Commer, A. A. Kornyshev, *J. Phys. Chem. B.* **2002**, *106*, 10560.
[17] A. A. Kornyshev, A. M. Kuznetsov, E. Spohr, J. Ulstrup, *J. Phys. Chem. B.* **2003**, *107*, 3351.
[18] M. K. Petersen, F. Wang, N. P. Blake, H. Metiu, G. A. Voth, *J. Phys. Chem. B.* **2005**, *109*, 3727.
[19] R. Paul, S. J. Paddison, *J. Chem. Phys.* **2005**, *123*, 224704.
[20] S. S. Jang, V. Molinero, T. Cagin, W. A. Goddard, *J. Phys. Chem. B.* **2004**, *108*, 3149.
[21] N. P. Blake, G. Mills, H. Metiu, *J. Phys. Chem. B.* **2007**, *111*, 2490.
[22] S. T. Cui, J. W. Liu, M. E. Selvan, S. J. Paddison, D. J. Keffer, B. J. Edwards, *J. Phys. Chem. B.* **2008**, *112*, 13273.
[23] C. K. Knox, G. A. Voth, *J. Phys. Chem. B.* **2010**, *114*, 3205.
[24] J. T. Wescott, Y. Qi, L. Subramanian, T. W. Capehart, *J. Chem. Phys.* **2006**, *124*, 134702.
[25] K. Malek, M. Eikerling, Q. P. Wang, Z. S. Liu, S. Otsuka, K. Akizuki, M. Abe, *J. Chem. Phys.* **2008**, *129*, 204702.
[26] J. A. Elliott, S. J. Paddison, *Phys. Chem. Chem. Phys.* **2007**, *9*, 2602.
[27] J. A. Asensio, E. M. Sánchez, P. Gómez-Romero, *Chem. Soc. Rev.* **2010**, *39*, 3210.
[28] Q. Li, J. O. Jensen, R. F. Savinell, N. J. Bjerrum, *Prog. Polym. Sci.* **2009**, *34*, 449.
[29] J. A. Asensio, P. Gomez-Romero, *Fuel Cells.* **2005**, *5*, 336.
[30] A. Buckley, D. E. Stuetz, G. A. Serad, "Polybenzimidazoles", in: *Encyclopedia of Polymer Science and Engineering*, H. F. Mark, Ed., John Wiley & Sons, New York **1988**, p. 572.
[31] B. Xing, O. Savadogo, *J. New Mat. Electrochem. Systems* **1999**, *2*, 95.
[32] M. Kawahara, J. Morita, M. Rikukawa, K. Sanui, N. Ogata, *Electrochim. Acta.* **2000**, *45*, 1395.
[33] T. Dippel, K. D. Kreuer, J. C. Lassegues, D. Rodriguez, *Solid State Ionics* **1993**, *61*, 41.
[34] R. P. Hamlen, E. J. Szymalak, *Electrochem. Technol.* **1966**, *4*, 172.
[35] J. S. Wainright, J. T. Wang, D. Wang, R. Savinell, M. Litt, *J. Electrochem. Soc.* **1995**, *142*, L121.
[36] J. Mader, L. Xiao, T. J. Schmidt, B. C. Benicewicz, *Adv. Polym. Sci.* **2008**, *216*, 63.
[37] Y. L. Ma, J. S. Wainright, M. H. Litt, R. F. Savinell, *J. Electrochem. Soc.* **2004**, *151*, A8.
[38] P. Musto, F. E. Karasz, W. J. Macknight, *Polymer* **1989**, *30*, 1012.
[39] X. Glipa, B. Bonnet, B. Mula, D. J. Jones, J. Roziere, *J. Mater. Chem.* **1999**, *9*, 3045.
[40] R. Bouchet, E. Siebert, *Solid State Ionics.* **1999**, *118*, 287.
[41] Q. Li, R. He, R. W. Berg, H. A. Hjuler, N. J. Bjerrum, *Solid State Ionics* **2004**, *168*, 177.
[42] C. E. Hughes, S. Haufe, B. Angerstein, R. Kalim, U. Mahr, A. Reiche, M. Baldus, *J. Phys. Chem. B.* **2004**, *108*, 13626.
[43] J. R. P. Jayakody, S. H. Chung, L. Durantino, H. Zhang, L. Xiao, B. C. Benicewicz, S. G. Greenbaum, *J. Electrochem. Soc.* **2007**, *154*, B242.
[44] N. W. Brooks, R. A. Duckett, J. Rose, I. M. Ward, J. Clements, *Polymer* **1993**, *34*, 4038.
[45] R. He, Q. Li, J. O. Jensen, N. J. Bjerrum, *J. Polym. Sci. Part A Polym. Chem.* **2007**, *45*, 2989.
[46] G. Scatchard, *Ann. N. Y. Acad. Sci.* **1949**, *51*, 660.
[47] S. Li, J. R. Fried, J. Colebrook, J. Burkhardt, *Polymer* **2010**, *51*, 5640.
[48] S. Li, J. R. Fried, J. Colebrook, *Polym. Eng. Sci.* **2013**, *53*, 597.
[49] S. Zhu, L. Yan, D. Zhang, Q. Feng, *Polymer* **2011**, *52*, 881.
[50] S. Pahari, C. K. Choudhury, P. R. Pandey, M. More, A. Venkatnathan, S. Roy, *J. Phys. Chem. B.* **2012**, *116*, 7357.
[51] S. Dapprich, I. Komaromi, K. S. Byun, K. Morokuma, M. J. Frisch, *J. Mol. Struc. Theochem.* **1999**, *461*, 1.
[52] T. Vreven, K. Morokuma, *J. Comput. Chem.* **2000**, *21*, 1419.
[53] B. H. Schlegel, J. M. Millam, S. S. Iyengar, G. A. Voth, A. D. Daniels, G. E. Scuseria, M. J. Frisch, *J. Chem. Phys.* **2001**, *114*, 9758.
[54] S. S. Iyengar, B. H. Schlegel, J. M. Millam, G. A. Voth, G. E. Scuseria, M. J. Frisch, *J. Chem. Phys.* **2001**, *115*, 10291.
[55] B. H. Schlegel, S. S. Iyengar, X. Li, J. M. Millam, G. A. Voth, G. E. Scuseria, M. J. Frisch, *J. Chem. Phys.* **2002**, *117*, 8694.
[56] S. S. Iyengar, H. B. Schlegel, G. A. Voth, J. M. Millam, G. E. Scuseria, M. J. Frisch, *Isr. J. Chem.* **2002**, *42*, 191.
[57] S. S. Iyengar, H. B. Schlegel, G. A. Voth, *J. Phys. Chem. A.* **2003**, *107*, 7269.
[58] S. S. Iyengar, M. J. Frisch, *J. Chem. Phys.* **2004**, *121*, 5061.
[59] N. Rega, S. S. Iyengar, G. A. Voth, H. B. Schlegel, T. Vreven, M. J. Frisch, *J. Phys. Chem. B.* **2004**, *108*, 4210.
[60] A. K. Rappe, C. J. Casewit, K. S. Colwell, W. A. Goddard, III, W. M. Skiff, *J. Am. Chem. Soc.* **1992**, *114*, 10024.
[61] Gaussian 03, Revision C.02, M. J. Frisch, G. W. Trucks, H. B. Schlegel, G. E. Scuseria, M. A. Robb, J. R. Cheeseman, J. A. Montgomery, T. Vreven, K. N. Kudin, J. C. Burant, J. M. Millam, S. S. Iyengar, J. Tomasi, V. Barone, B. Mennucci, M. Cossi, G. Scalmani, N. Rega, G. A. Petersson, H. Nakatsuji, M. Hada, M. Ehara, K. Toyota, R. Fukuda, J. Hasegawa, M. Ishida, T. Nakajima, Y. Honda, O. Kitao, H. Nakai, M. Klene, X. Li, J. E. Knox, H. P. Hratchian, J. B. Cross, V. Bakken, C. Adamo, J. Jaramillo, R. Gomperts, R. E. Stratmann, O. Yazyev, A. J. Austin, R. Cammi, C. Pomelli, J. W. Ochterski, P. Y. Ayala, K. Morokuma, G. A. Voth, P. Salvador, J. J. Dannenberg, V. G. Zakrzewski, S. Dapprich, A. D. Daniels, M. C. Strain, O. Farkas, D. K. Malick, A. D. Rabuck, K. Raghavachari, J. B. Foresman, J. V. Ortiz, Q. Cui, A. G. Baboul, S. Clifford, J. Cioslowski, B. B. Stefanov, G. Liu, A. Liashenko, P. Piskorz, I. Komaromi, R. L. Martin, D. J. Fox, T. Keith, M. A. Al-Laham, C. Y. Peng, A. Nanayakkara, M. Challacombe, P. M. W. Gill, B. Johnson, W. Chen, M. W. Wong, C. Gonzalez, J. A. Pople, Gaussian, Inc., Wallingford CT, **2004**.
[62] S. Li, J. R. Fried, J. Sauer, J. Colebrook, D. S. Dudis, *Int. J. Quantum Chem.* **2011**, *111*, 3212.
[63] A. D. McNaught, A. Wilkinson, *Compendium of Chemical Terminology*, 2nd edition Blackwell Scientific Publications, Oxford **1997**.

[64] A. Einstein, O. Stern, *Ann. Phys. (Leipzig).* **1913**, *40*, 551.
[65] J. W. Ochterski, *Thermochemistry in Gaussian, Gaussian, Inc*, Wallingford, CT **2000**.
[66] F. B. van Duijneveldt, J. G. C. M. van Duijneveldt-van de Rijdt, J. H. van Lenthe, *Chem. Rev.* **1994**, *94*, 1873.
[67] D. Young, *Computational Chemistry. A Practical Guide for Applying Techniques to Real World Problems*, 1st edition, John Wiley & Sons, Inc., New York, NY **2001**, p. 408.
[68] C. Peng, P. Y. Ayala, H. B. Schlegel, M. J. Frisch, *J. Comp. Chem.* **1996**, *17*, 49.
[69] C. Peng, H. B. Schlegel, *Israel J. Chem.* **1994**, *33*, 449.
[70] M. J. S. Dewar, S. Kirschner, *J. Am. Chem. Soc.* **1971**, *93*, 4292.
[71] Gaussian 09, Revision A.1, M. J. Frisch, G. W. Trucks, H. B. Schlegel, G. E. Scuseria, M. A. Robb, J. R. Cheeseman, G. Scalmani, V. Barone, B. Mennucci, G. A. Petersson, H. Nakatsuji, M. Caricato, X. Li, H. P. Hratchian, A. F. Izmaylov, J. Bloino, G. Zheng, J. L. Sonnenberg, M. Hada, M. Ehara, K. Toyota, R. Fukuda, J. Hasegawa, M. Ishida, T. Nakajima, Y. Honda, O. Kitao, H. Nakai, T. Vreven, M. A. J. Jr., J. E. Peralta, F. Ogliaro, M. Bearpark, J. J. Heyd, E. Brothers, K. N. Kudin, V. N. Staroverov, R. Kobayashi, J. Normand, K. Raghavachari, A. Rendell, J. C. Burant, S. S. Iyengar, J. Tomasi, M. Cossi, N. Rega, J. M. Millam, M. Klene, J. E. Knox, J. B. Cross, V. Bakken, C. Adamo, J. Jaramillo, R. Gomperts, R. E. Stratmann, O. Yazyev, A. J. Austin, R. Cammi, C. Pomelli, J. W. Ochterski, R. L. Martin, K. Morokuma, V. G. Zakrzewski, G. A. Voth, P. Salvador, J. J. Dannenberg, S. Dapprich, A. D. Daniels, Ö. Farkas, J. B. Foresman, J. V. Ortiz, J. Cioslowski, D. J. Fox, Gaussian, Inc., Wallingford CT, **2009**.
[72] W. Humphrey, A. Dalke, K. Schulten, *J. Mol. Graph.* **1996**, *14*, 33.
[73] J. A. Asensio, S. Borrós, P. Gómez-Romero, *Electrochem. Commun.* **2003**, *5*, 967.
[74] R. R. Dogonadze, *The Chemical Physics of Solvation*, (3 vols. ed.), Elsevier, Amsterdam **1985**.
[75] R. Bianco, S. Wang, J. T. Hynes, *Advances in Quantum Chemistry, Vol. 55, Applications of Theoretical Methods to Atmospheric Science*, Academic Press, Oxford, UK **2008**, p. 387.